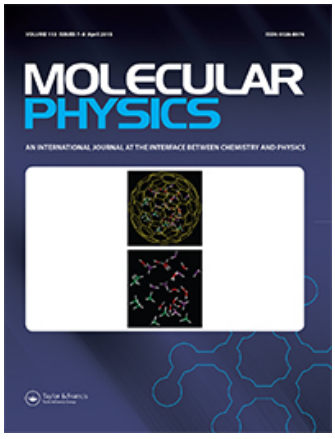

Molecular Physics: An International Journal at the Interface Between Chemistry and Physics
Publication details, including instructions for authors and subscription information:
http://www.tandfonline.com/loi/tmph20

Infrared spectroscopy of solid mixed ammonia-water and acetylene-water aerosol particles

Merrill Isenor[ab] & Ruth Signorell[ab]
[a] Department of Chemistry, University of British Columbia, Vancouver, Canada
[b] Laboratory of Physical Chemistry, ETH Zurich, Zurich, Switzerland
Published online: 18 Nov 2014.

To cite this article: Merrill Isenor & Ruth Signorell (2015) Infrared spectroscopy of solid mixed ammonia-water and acetylene-water aerosol particles, Molecular Physics: An International Journal at the Interface Between Chemistry and Physics, 113:8, 823-834, DOI: 10.1080/00268976.2014.981232

To link to this article: http://dx.doi.org/10.1080/00268976.2014.981232

Molecular Physics, 2015
Vol. 113, No. 8, 823–834, http://dx.doi.org/10.1080/00268976.2014.981232

RESEARCH ARTICLE

Infrared spectroscopy of solid mixed ammonia–water and acetylene–water aerosol particles

Merrill Isenor[a,b] and Ruth Signorell[a,b,*]

[a]*Department of Chemistry, University of British Columbia, Vancouver, Canada;* [b]*Laboratory of Physical Chemistry, ETH Zurich, Zurich, Switzerland*

(*Received 11 September 2014; accepted 22 October 2014*)

Mixed water aerosols are important components of planetary and lunar atmospheres. In this work, we use rapid-scan Fourier transform infrared (IR) spectroscopy to study solid ammonia–water and acetylene–water aerosol particles formed in a bath gas cooling cell at 78 K. With this set-up, we record time-dependent extinction spectra of particle ensembles in the mid-IR to monitor changes to the internal structure of the aerosol particles. Both ammonia–water and acetylene–water were found to form molecularly mixed structures. The mixing is observed by monitoring the profile for the ammonia ν_2 band and the acetylene ν_5 band, both of which are sensitive to particle properties. Depending on the injection conditions, the mixed particles form either immediately after sample injection or after a short mixing period of several tens of minutes. We confirm the formation of mixed particles by comparing the experimental spectra with spectra calculated with the vibrational exciton model.

Keywords: vibrational exciton model; molecular ices; solid-state diffusion

1. Introduction

There is considerable interest in the composition of the atmospheres of planets and moons in our solar system with mixed aerosols as important components. The infrared (IR) spectra of aerosol particles can be sensitive to intrinsic particle properties, such as particle size, shape, architecture, and structure [1–3]. This makes IR spectroscopy a useful method to study the properties of aerosol particles, for example, by monitoring temporal changes of band shapes, which can arise from changes in the particle morphology or internal structure (e.g. mixing and demixing in multicomponent particles).

In this work, we present time-dependent Fourier transform infrared (FTIR) extinction (absorption + scattering) spectra for solid ammonia–water and acetylene–water aerosol particles formed in a bath gas cooling cell at 78 K. Both of these types of mixed particles may be important throughout our solar system. Recent analysis of near-IR spectra collected during Saturn's Great Storm of 2010–2011 has found evidence of multi–component aerosol particles partially composed of ammonia and water ice [4]. Both water ice and ammonia ice clouds exist in the atmospheres of Jupiter, Uranus, and Neptune [5,6]. Additionally, the analysis of the water plumes on Enceladus has found small amounts of ammonia and acetylene [7,8].

Water ice is a major component of many astrophysical ices. As a result, thin films of a variety of water ice mixtures have been widely examined in the IR [9,10], including ammonia–water [9–24] and acetylene–water [10,25–27] thin films. The IR spectra of aerosol particles may vary greatly from those of the bulk mixtures due to the size and shape of particles [1–3, 28] and these differences must be considered when analysing the spectra of aerosol particles. As well, experiments in the particle phase are required to determine possible particle architectures (e.g. core–shell particles) as these properties cannot be determined from thin film measurements.

We have previously studied other binary mixed aerosol particles containing water, ammonia, or acetylene that may be relevant for astrophysical studies, such as acetylene–carbon dioxide particles [29,30], ammonia–acetylene particles [31], and water–carbon dioxide particles [32]. While all these experiments were performed under similar conditions, each of the binary mixed aerosol systems was found to have different shapes, architectures, and internal structures. These different particle properties can have a dramatic effect on the band shapes in the IR spectra. Acetylene and carbon dioxide were found to immediately form metastable co–crystalline aerosol particles that decomposed to pure acetylene and pure carbon dioxide with time [29,30]. In contrast, acetylene formed a co-crystal with ammonia via solid-state diffusion after the initial formation of core–shell particles [31]. The study of water–carbon dioxide aerosol particles showed no evidence of molecular mixing. A plausible structure for water–carbon dioxide particles is that of solid water particles partially engulfed by patches of

* Corresponding author. Email: rsignorell@ethz.ch

solid carbon dioxide [32]. These examples demonstrate that the exact architecture and structure for aerosol particles is highly dependent on the types of molecules present and their specific intermolecular interactions.

In this work, we first present our study of solid ammonia–water aerosol particles (Section 3.1) followed by the results for the acetylene–water aerosol particles (Section 3.2). We focus the majority of our analysis on the ammonia–water particles since we observe similar results for both ammonia–water and acetylene–water particles. Additionally, there appears to be greater astrophysical interest in ammonia–water mixtures. We compare our particle spectra to literature spectra of thin film mixtures and to calculated extinction spectra using the vibrational exciton model to confirm our interpretations of the IR spectra.

2. Methods

2.1. Experiments

All experiments were performed in a bath gas cooling cell. A complete description of the experimental set-up can be found elsewhere [33]. The cell was cooled to 78 K with liquid nitrogen and filled with 500 mbar of helium. Ammonia–water and acetylene–water aerosol particles were generated by injecting room temperature sample gases (ammonia: 200 or 400 ppm, acetylene: 220 ppm, water: 640–1200 ppm, all in helium; total sample pressure: 2 bar) into the cell by opening two separate magnetic valves. The injection of dilute room temperature gases into the cold cell leads to supersaturation and aerosol particle formation. Valve opening times were typically 900 ms. We use the term 'premixed injection' if the two gases are first premixed and then injected into the cell through a single valve. Both valves are used in order to inject the two different sample gases. To inject one gas after the other, a delay can be introduced between the opening times of each valve. The delay time between opening the first valve and opening the second valve was typically 1000 ms. We refer to this type of injection as 'sequential injection' throughout the paper. If both valves are opened at the same time (i.e. no delay), we use the phrase 'simultaneous injection'. (Note that in this study, we find the same results for both the premixed and simultaneous injection methods.)

A Bruker IFS66v/S rapid-scan FTIR spectrometer (∼380 ms per scan at 0.5 cm^{-1} spectral resolution) was used to collect spectra of the aerosol particles suspended in the cell for a time period of 30–120 minutes after injection. Immediately after injection, we collect spectra that consist of only a single scan to achieve the best time resolution for spectra. As the measurement time progresses and particles begin to move out of the path of the IR beam, we average multiple scans to improve the signal-to-noise ratio in the spectra.

2.2. Vibrational exciton calculations

The vibrational exciton model was used to calculate band shapes in IR extinction spectra for the ammonia and acetylene aerosol particles. A detailed description of this model can be found elsewhere [1,34–37]. Briefly, it is a quantum mechanical model to calculate the IR extinction spectra for molecular nanoparticles. It has been previously shown that for vibrations with a transition dipole moment greater than 0.1 D, the dominant contribution to the IR band shape is resonant dipole coupling (exciton coupling) [1,34–45]. This coupling lifts the degeneracy of the uncoupled molecular vibrational states and leads to vibrational eigenfunctions that are delocalised over the particle. The result is highly structured band shapes that depend strongly on intrinsic particle properties (size, shape, architecture, and composition). In the exciton model, the vibrational Hamiltonian is essentially reduced to this dominant contribution which reduces the computational cost required to calculate spectra and allows for the calculation of spectra for particles containing tens of thousands of molecules.

The input parameters required for the calculations are the transition dipole moment, the molecular vibrational frequency, and the molecular structure. Calculations were performed for pure crystalline (cubic structure) and amorphous ammonia particles for the ammonia ν_2 band. The amorphous structure was used as a proxy for the molecularly mixed water–ammonia particles since in both cases, the ammonia molecules are disordered within the particles. The vibrational frequency for the ammonia ν_2 band was set to 1060 cm^{-1} for the pure crystalline particles and the transition dipole moment was set to 0.21 D [42]. The vibrational frequency for the amorphous ammonia particles was shifted from 40 to 1100 cm^{-1} corresponding to the shift calculated for the ammonia monomer and the ammonia–water 1:1 complex [46]. Octahedral particles were chosen for the crystalline ammonia calculations based on the experimental observations of ammonia particle morphology by Pope *et al*. [47]. Spherical particles were used for the amorphous ammonia particles since this is the most likely shape for an amorphous structure. It is noteworthy that spectra of amorphous particles are largely insensitive to the particle shape.

The calculated acetylene spectra were taken from previous work in our group [48]. The calculations performed for the acetylene ν_5 band (transition dipole = 0.28 D) for pure polycrystalline particles were derived from an orthorhombic crystal structure. (Note that we found pure acetylene particles to be stable in a polycrystalline form rather than in the crystalline form.) The amorphous acetylene structure taken from the work of Preston *et al*. [48] is used to approximate the mixed acetylene–water particles. Non-crystalline particles are most likely to be spherical, thus spherical particles were used in the calculations for both the polycrystalline and the amorphous acetylene particles. The input

frequency for the pure acetylene particle was 772 cm^{-1}. This value was shifted to 793 cm^{-1} for the amorphous particle calculation based on the observed experimental frequency for the 1:1 acetylene–water complex [49].

3. Results

The size of aerosol particles formed in the cooling cell depends on the exact experimental conditions (e.g. temperature and pressure of the bath gas in the cell and the concentration of sample gases injected into the cell) [34,40,42,43,50]. The size of aerosol particles can be estimated from their IR spectra and a detailed summary of the effects of particle size on IR spectra can be found in the paper by Sigurbjörnsson *et al*. [1]. We estimate that the particles studied in this work are in the order of 10–100 nm in diameter. The lack of elastic scattering in any of our spectra (which would be visible as a sloping baseline and dispersive band shapes, e.g. Figures 2 and 3 in Isenor *et al*. [32]) provides an upper limit of 100 nm for the particle diameters. Below 10 nm, the band profiles are highly dependent on the particle size, while between 10 and 100 nm, the spectra are essentially independent of the size [1]. We have injected different sample gas concentrations into the cell (while keeping the bath gas temperature and pressure constant) without any marked differences in the band profiles in spectra. Thus, we estimate a lower limit to the particle diameter in general of 10 nm.

3.1. *Ammonia–water aerosol particles*

3.1.1. *Overview of aerosol particle IR spectra*

Experimental IR spectra of pure solid ammonia and water aerosol particles (traces (a) and (b), respectively) and mixed ammonia–water aerosol particles (traces (d) and (e)) are presented in Figure 1. This figure provides an overview of the extinction for each type of particles in the mid-IR range at 78 K. A series of spectra were collected over a period of 30 minutes after sample injection. No changes were observed in any of the spectra during this time. Table 1 provides a summary of the band positions determined at the band maxima for the pure and mixed ammonia and water particle spectra shown in Figure 1.

The spectrum of pure ammonia ice aerosol particles is depicted in Figure 1(a). Solid ammonia aerosol particles have a cubic structure based on comparison to IR spectra from previous aerosol studies [31,42] and thin films of crystalline ammonia [51]. We focus the majority of our analysis on the ν_2 bending mode at 1066 cm^{-1}, which is often referred to as the 'umbrella' motion. This band is sensitive to the size, shape, structure, and architecture of particles [42,52]. The other bands in the pure ammonia spectrum are the ν_4 band at 1642 cm^{-1} (a bending motion), the ν_1 and ν_3 stretching modes at 3213 and 3378 cm^{-1}, respectively, and the $\nu_2 + \nu_6$ combination band (ν_6 is a lattice vibration [53]). A spectrum of pure water ice particles is shown in trace (b). The shape of the OH stretching band suggests that the water particles are likely amorphous [54]. The broad band from 600–1000 cm^{-1} is the libration mode (lattice vibration), the ν_2 band at 1650 cm^{-1} is the bending mode, and the broad band from 3000–3600 cm^{-1} is the region of the ν_1 and ν_3 stretching modes. The small peak at 3698 cm^{-1} is referred to as the 'dangling-OH' band. It results from free OH at the surface of the particles not involved in hydrogen bonding [55]. A sum spectrum of the pure ammonia spectrum (trace (a)) and pure water spectrum (trace (b)) is shown in trace (c). The ratio of H_2O:NH_3 is roughly 2:1. The sum spectrum demonstrates which features would be expected for an ensemble that consists of

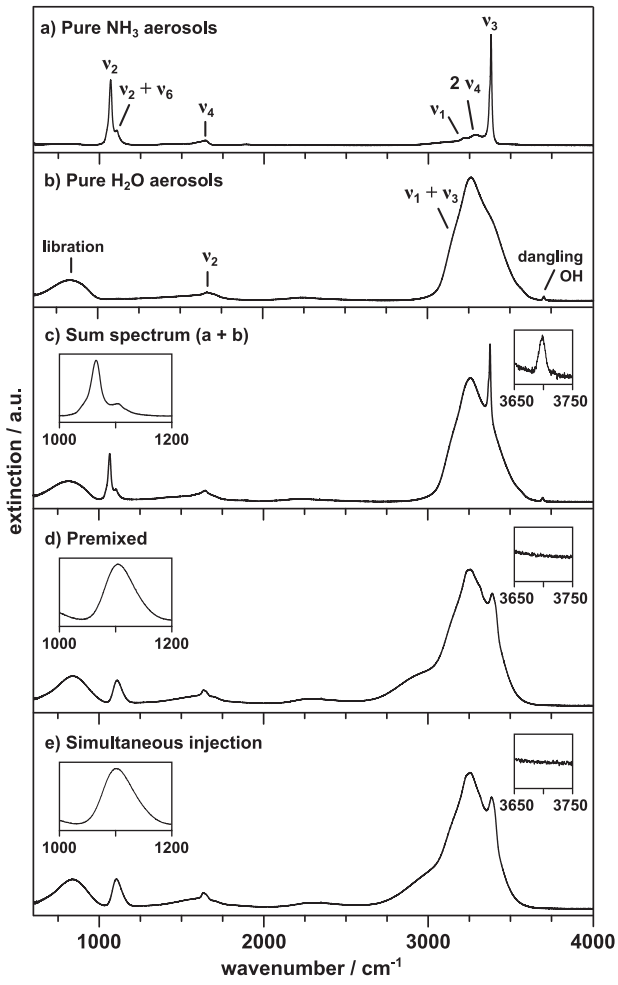

Figure 1. Overview infrared aerosol particle spectra for (a) pure NH_3, (b) pure H_2O, (c) a sum spectrum (addition of spectrum (a) and spectrum (b)), (d) particles formed after injection of a premixed H_2O/NH_3 sample, and (e) particles formed after simultaneous injection of NH_3 and H_2O samples. Insets in (c), (d), and (e) show an expanded view of the ammonia ν_2 band and the dangling-OH stretch region. The ratio of H_2O:NH_3 is approximately 2:1 in (c), (d), and (e).

Table 1. Infrared band assignments for pure and mixed NH_3 and H_2O aerosol particles formed in the cooling cell (see Figure 1).

		Position (cm^{-1})	
	Band	Pure	Mixed*
NH_3	ν_2	1066	1100§
	$\nu_2 + \nu_6$	1104	§
	ν_4	1642	1631†
	ν_1	3213	†
	$2\nu_4$	3287	†
	ν_3	3378	3383†
H_2O	Libration	814	833
	ν_2	1650	1631†
	$\nu_1 + \nu_3$	3257	3253†
	Dangling-OH	3698	–

*Taken from spectra recorded after simultaneous injection of the sample gases.
§NH_3 ν_2 and $\nu_2 + \nu_6$ overlap.
†H_2O and NH_3 overlap in this region.

pure ammonia and pure water particles; i.e. with no mixing of the two substances on a molecular level.

Figure 1(d) and 1(e) both show spectra for mixed ammonia–water particles, i.e. with mixing of the two substances on a molecular level. The ratio H_2O:NH_3 is approximately 2:1 for both experiments. This ratio was calculated using the integrated band intensities of the spectra along with the band strengths determined at 10 K for thin films of water and ammonia (taken from the work of d'Hendecourt and Allamandola [9]). The spectrum in Figure 1(d) was recorded immediately after injection of a premixed ammonia/water gas sample (premixed injection), while the spectrum in Figure 1(e) was recorded immediately after simultaneous injection of each of the pure gas samples. These two spectra are almost identical. There are, however, pronounced differences between the sum spectrum (trace (c)) and theses two mixed spectra. The most notable difference occurs in the region of the ammonia umbrella mode (see insets), which is broadened and its position is shifted from 1066 to 1100 cm^{-1} for the mixed particles. Other changes in the spectra of the mixed particles include a broadening at the base of the OH stretch region (down to ~2600 cm^{-1}), a broadening and shift of the NH stretch band, and the loss of the dangling-OH band (see insets). In the following Sections 3.1.2 and 3.1.3, we provide evidence that the mixed particles (traces (d) and (e)) are amorphous with ammonia and water mixed on a molecular level.

3.1.2. *Comparison to thin film spectra*

Ammonia and water can form non-stoichiometric molecularly mixed solids or one of the possible hydrate structures: the hemihydrate ($2NH_3$–H_2O) [56], the monohydrate (NH_3–H_2O) [57], and the dihydrate (NH_3–$2H_2O$) [58]. The distinction between the non-stoichiometric ices and the hydrates relates to the hydrogen bonding in the solids, which is ordered in the case of the latter. Co-deposition of ammonia and water gases around 78 K will typically form amorphous mixed films. The hydrates may then be formed by annealing the amorphous films, provided that the film has the appropriate stoichiometry [11–14]. IR spectra exist for thin films of various ammonia–water mixtures [9–11,15,16], as well as for the hemihydrate [11–13,17–22], the monohydrate [11,14,17–19,23,24], and the dihydrate [13]. Several of these references include spectra of deuterated water or deuterated ammonia to avoid the overlap of the ammonia NH stretching region and the water OH stretching region.

In Figure 2, we compare the spectra of mixed particles with thin film measurements that have been previously published and made available for download [11,59]. Figure 2(a) and 2(b) both show our experimental spectra for mixed ammonia-water particles, with H_2O:NH_3 ratios of approximately 2:1 and 5:1, respectively. The different ratios were obtained by varying the amount of ammonia injected into the cell while keeping the amount of water constant. The main differences in these two spectra relate to moderate difference in the intensity of the ammonia features. Apart from that, very similar band profiles are observed for both mixing ratios. The IR spectra in traces (c)–(e) are thin film measurements for a 5:1 mixture, the monohydrate, and the hemihydrate, respectively, from Hudson and co-workers [11,59]. The spectra were recorded at 90 K for the ammonia–water film and 95 K for the monohydrate and hemihydrate thin films. The broad features above ~2000 cm^{-1} for the thin film spectrum of the 5:1 mixture (trace (c)) may be due to artefacts inherent to thin film measurements. For this reason, we focus our comparisons to the region between 600 and 2000 cm^{-1}.

The insets in Figure 2 show the region of the ammonia ν_2 band for each spectrum. The features in the particle spectra are quite similar to those for the 5:1 thin film in this region. The spectra of the hydrates, by contrast, are much more structured in the region of the H_2O libration band, the NH_3 umbrella band, and in the region where the ammonia ν_4 and water ν_2 bands overlap. Such strongly structured bands would be expected for the hydrates due to their ordered molecular structure. For molecularly mixed substances without any long-range order, however, one expects to observe broad rather featureless bands, such as the bands in traces (a)–(c). While not shown here, our NH_3–H_2O particle spectra also bear a strong resemblance to the 3:1 thin film measurement at 10 K by d'Hendecourt and Allamandola [9] and the 5:1 thin film measurement at 70 K by Knacke *et al*. [16]. These comparisons clearly indicate that the particles consist of ammonia and water molecules that are mixed on a molecular level but do not form hydrates. We would expect the formation of amorphous particles at 78 K based on the formation of amorphous films at similar temperatures. Additionally, we do not anneal the particles,

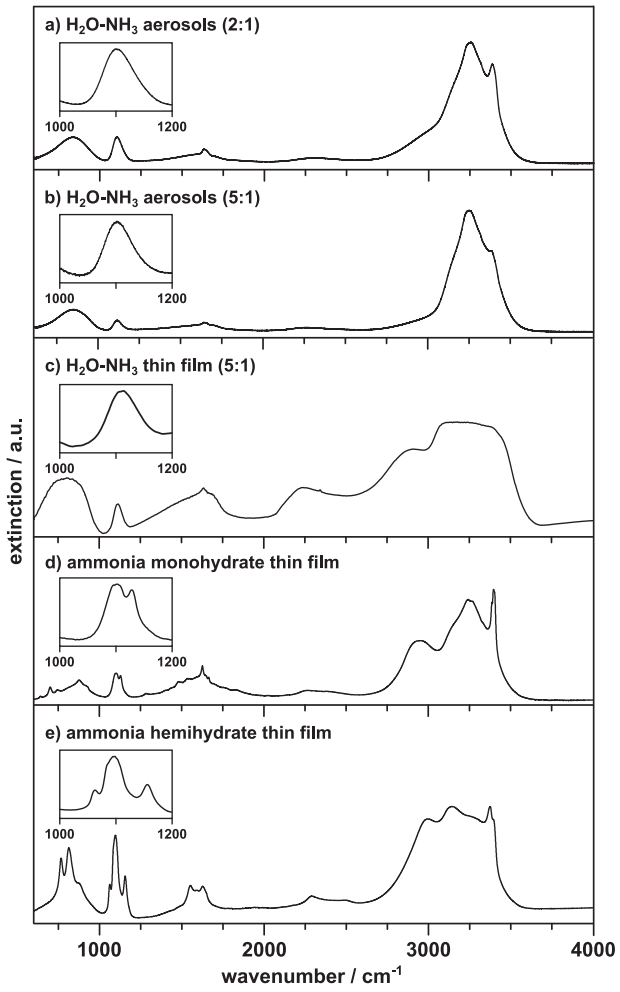

Figure 2. Comparison of NH_3–H_2O aerosol particle spectra to thin film spectra. (a) and (b) Molecularly mixed H_2O–NH_3 particles formed at 78 K after simultaneous injection of the sample gases, (c) H_2O–NH_3 thin film measurement at 90 K, (d) monohydrate thin film measurement at 95 K, and (e) hemihydrate thin film measurement at 95 K. Insets show an expanded view of the umbrella region. Thin film measurements were taken from the work of Hudson and co-workers [11,59]. All spectra are scaled to the same maximum for ease of comparison.

which is the usual procedure for forming crystalline thin films.

3.1.3. *Comparison to other particle spectra*

We are not aware of any previous studies of free ammonia–water aerosol particles, though previously Devlin *et al.* have examined ammonia–water ice particles collected on a cold window with IR spectroscopy. These results are summarised in two publications. In the first one, they studied the conversion of water ice nanocrystals to the crystalline ammonia monohydrate with saturated pressures of ammonia at 120 K [60]. In the second study, they focused on NH_3–D_2O systems to avoid overlap between the ammonia

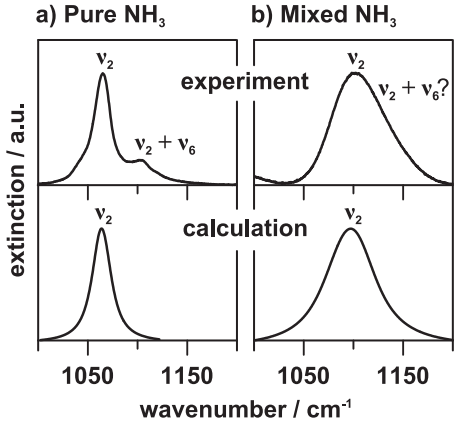

Figure 3. Comparison of experimental spectra and calculated spectra for (a) pure crystalline ammonia aerosol particles and (b) mixed amorphous ammonia–water aerosol particles.

and water bands and monitored the conversion of water ice particles to the monodeuterate (T = 115–123 K) and hemideuterate (T = 102–110 K) after exposure to ammonia vapour [22]. For the monohydrate (and monodeuterate) particles, the ammonia ν_2 band and the OH/OD-stretching bands again have much more structure than what we observe for our ammonia–water particles at 78 K [22,59]. In the hemideuterate studies, the focus was mainly on the OD-stretching band, which is strongly structured for experiments carried out at 107–110 K, indicating a crystalline deuterate structure (at 102 K, the resulting particles are assigned to an amorphous structure based on the observed broad bands) [22]. Again, there is much greater structure observed in the OD-stretching region for the deuterate spectra compared to the broad bands in our mixed ammonia–water aerosol particle spectra. Again, this is a clear indication that our particles are not hydrates.

It is also worthwhile to briefly compare the ammonia–water aerosol spectra with spectra of ammonia–acetylene particles, which were previously measured and analysed in our group [31]. The latter were found to have a co-crystalline structure. The ammonia ν_2 band in the ammonia–acetylene co-crystal observed at 1093 cm^{-1} is quite narrow, similar to the pure ammonia ν_2 band at 1067 cm^{-1}. This is in contrast to the broad band we observe for our ammonia–water aerosol particles at the same temperature and further indicates that the ammonia–water particles do not have any long-range order.

3.1.4. *Comparison to calculated spectra*

In order to confirm our experimental results that indicate the formation of molecularly mixed aerosol particles without long-range order, we have performed vibrational exciton calculations for different ammonia particle structures. Calculations were performed for pure cubic and amorphous ammonia particles (Section 2.2). Figure 3 shows the

comparison between experimental and calculated spectra in the region of the ammonia ν_2 band. The experimental spectrum of pure ammonia (panel (a)) closely matches the calculated spectrum for an octahedral ammonia particle with a cubic crystal structure. (Note that the experimental spectrum also shows the $\nu_2 + \nu_6$ combination band at 1104 cm^{-1}, which is not included in the simulation.) There is also very good agreement between the experimental ammonia–water spectrum and the calculated amorphous spectrum in panel (b). Both show a similarly broad unstructured band, which is by a factor of ~2.5 broader compared with the band of the crystalline particle. This further confirms that we form molecularly mixed amorphous (non-hydrate) ammonia–water aerosol particles immediately after injection of a premixed sample or simultaneous injection of the two sample gases.

3.1.5. *Mixing in core–shell ammonia–water particles*

For both the premixed and simultaneous injection measurements shown in Figure 1, the mixed particles were already formed by the time we record the first spectrum (i.e. <1 s). As mentioned, a series of spectra were recorded for a further 30 minutes after injection. During this time, no changes were observed in the spectra of either the pure particles or the mixed particles. To investigate how fast mixing of pure solid ammonia and pure solid water occurs, we measured spectra for aerosol particles formed after sequential injection of ammonia and water into the cell. The sequential injection initially forms core–shell particles with the substance injected first forming the core and the substance injected second forming the shell. We can then observe changes to the spectra with time due to the mixing of the two substances via solid-state diffusion.

Time-resolved spectra from two sequential measurements with an H_2O:NH_3 ratio of ~2:1 are shown in Figure 4 in the region of the ammonia ν_2 mode. The spectra in Figure 4 are scaled to the same maximum to facilitate comparison of the band profiles. (Note that during the 30 minute measurement, particles gradually move towards the walls of the cell and out of the path of the IR beam, leading to a gradual decrease in signal intensity.) Panel (a) shows spectra from an experiment where water was injected first while panel (b) shows spectra from an experiment where ammonia was injected first. In both cases, some mixing has already started by the time we record the first spectrum (which is immediately after injection of the second gas sample). Therefore, the first spectra contain features of the pure crystalline substances (Figure 1(a)–(c)) together with features of the molecularly mixed particles (Figure 1(d) and 1(e)). Over time, there is an evolution of the ammonia ν_2 band shape more and more toward that of the molecularly mixed particles for both injection orders. As a result, the broad band at 1100 cm^{-1} gains intensity and the narrower band at 1066 cm^{-1} loses intensity over time. While the spectra in

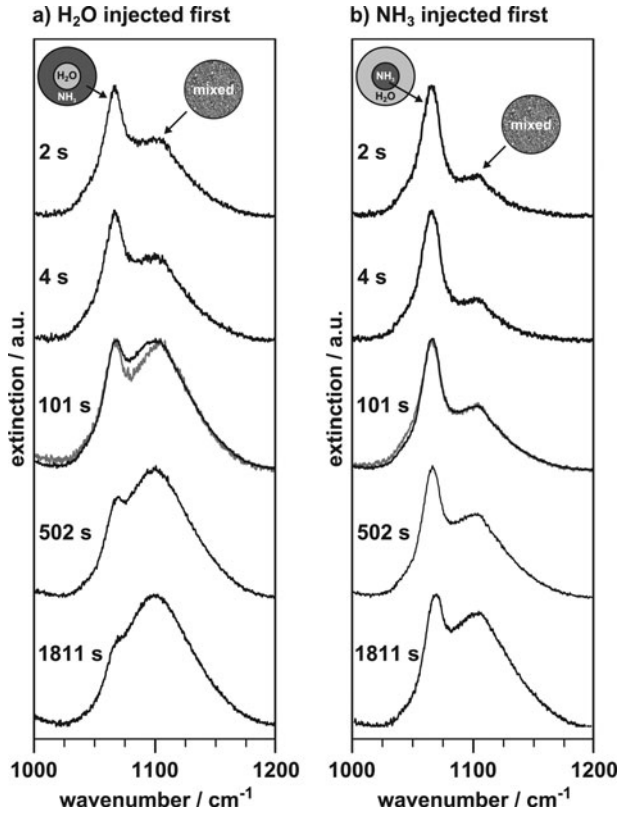

Figure 4. Temporal evolution in the region of the ammonia umbrella mode after sequential injection of the sample gases. The injection orders were: (a) H_2O then NH_3 and (b) NH_3 then H_2O. All other injection conditions remained the same for both experiments. The ratio of H_2O:NH_3 is approximately 2:1. Examples of fitting results used to create the plots in Figure 6 are shown for the spectra recorded at 101 s (grey traces).

Figure 4 approach the broad ν_2 band of the mixed state, the signature of the pure crystalline state at 1066 cm^{-1} does not completely disappear within the 30 minute experiment. This experiment was repeated and spectra were monitored for 120 minutes after injection (not shown). Even during this longer time frame, the spectra never reached the fully mixed state seen in the simultaneous and premixed spectra (Figure 1(d) and 1(e)). The amount of further mixing after 30 minutes was found to be minimal. We think that during the sequential injections a certain fraction of pure ammonia particles (and also pure water particles) are formed, which cannot mix by solid-state diffusion (see discussion further below). These pure particles are likely responsible for the sudden stop of the mixing process. The extent of mixing can also be determined by examining changes to the band profiles in the region of the OH and NH stretching motions in the sequential measurements (not shown). With time, the OH stretching band evolves toward the profile observed in Figure 1(d) and 1(e) – namely, a broadening of the band at the base. Also, the NH stretching band broadens with time and becomes less prominent. In addition, a decrease in the intensity of the water dangling-OH band is observed (not

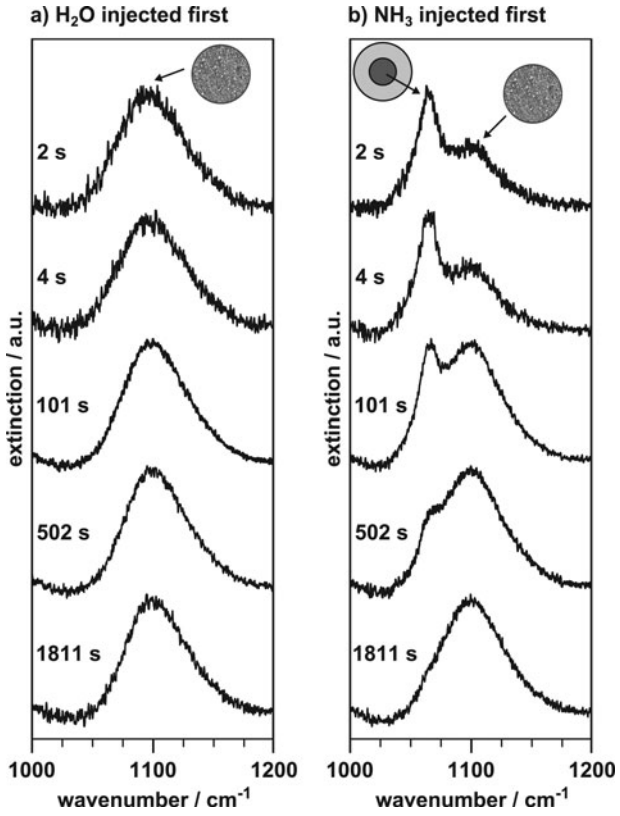

Figure 5. As for Figure 4, but with a ratio of H_2O:NH_3 of approximately 5:1.

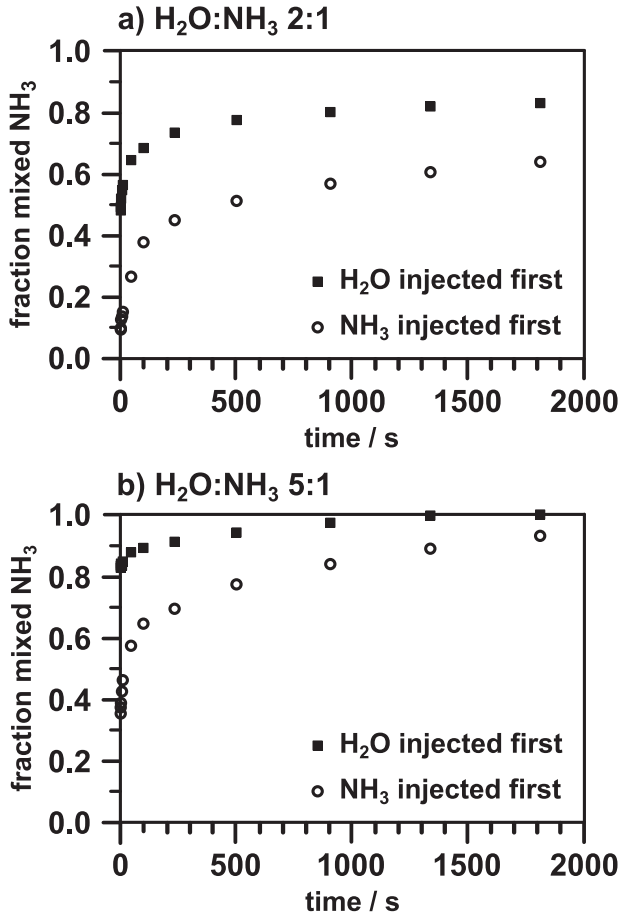

Figure 6. Fraction of molecularly mixed NH_3 as a function of time for particles formed by sequential injection. The ratio of H_2O:NH_3 is approximately (a) 2:1 and (b) 5:1. The corresponding spectra are shown in Figures 4 and 5, respectively. Sample fits are depicted in Figure 4 (grey traces) for spectra recorded 101 s after injection.

shown). Devlin and Uras [22] previously used the decrease and disappearance of this band in IR spectra (referred to in their case as 'dangling-D' since they used D_2O in measurements) to indicate the coating of D_2O nanocrystals with ammonia.

To examine the effect of the ratio of H_2O:NH_3 on the mixing kinetics, the experiments shown in Figure 4 were repeated with a H_2O:NH_3 ratio of approximately 5:1 (which corresponds to the simultaneous measurement in Figure 2(b)). For these experiments, the concentration of the water gas sample remained constant while a lower concentration was used for the ammonia gas sample. The results for these experiments are presented in Figure 5 in an analogous manner to the spectra in Figure 4. The evolution of the bands with time is very similar to those observed for the 2:1 ratio. The difference to Figure 4 is that everything happens faster in Figure 5 and that mixing almost goes to completion after 30 minutes. Faster mixing is to be expected for the 5:1 ratio because the ammonia shell (trace (a)) is thinner and the ammonia core (trace (b)) is smaller compared to the 2:1 mixture. A lower ammonia content obviously also results in a much lower fraction of pure ammonia particles (most ammonia is bound in core–shell particles).

Fitting the spectral band shapes allows us to quantify the extent of molecular mixing in the ammonia–water aerosol particles. We analysed the fraction of mixing for both the 2:1 and 5:1 H_2O:NH_3 aerosol particle measurements (Figures 4 and 5, respectively). A linear combination of the pure (Figure 1(a)) and mixed (Figure 2(a) and 2(b)) band shapes were fitted to the experimental spectra. We assumed the spectra after simultaneous injection to represent the case where the particles have the maximum extent of mixing since there were no further changes to these spectra with time. Examples of fitted spectra are shown in Figure 4 for the spectra recorded 101 s after injection (grey traces). The plots in Figure 6 show the fraction of mixed ammonia as a function of time for both injection orders. (It is important to note that the mixing fraction in the figures is not the same as the mole fraction since the extinction coefficients for the ν_2 band in pure and mixed ammonia are not equal (see, for example, the work by d'Hendecourt and Allamandola [9] of band strengths for the ν_2 band in pure ammonia and a 3:1 water–ammonia mixture)). The data in Figure 6(a) corresponds to the 2:1 spectra (Figure 4),

while the plot in Figure 6(b) corresponds to the 5:1 spectra (Figure 5). Both mixing ratios show similar trends with time. Mixing is fast in the first 300 s after injection, and then begins to level off. For both concentration ratios, the extent of mixing is greater when water is injected first, though the difference between the injection orders is less pronounced when the concentration of ammonia is lower. The fraction of molecularly mixed ammonia reaches the greatest value when less ammonia is present in the aerosol particles.

We suspect the fact that the onset of mixing always occurs sooner when water is injected first and also proceeds to a more fully mixed state may be related to the different melting points of water and ammonia (273.15 and 195.41 K, respectively, at 1 atm). When water is injected first, it freezes and forms solid aerosol particles already in the lower part of the injection tube just before the entrance into the actual cell (see Figure 1 in Lang *et al*. [33]). These water particles could then act as nucleation sites for the ammonia gas because the ammonia is not likely to freeze in the inlet tube due to its lower melting point. This leads to the formation of predominantly core–shell particles and not the formation of a substantial fraction of pure ammonia and pure water particles. Molecular mixing would then proceed via solid-state diffusion in these core–shell particles. It has been previously shown that ammonia on the surface of water particles can diffuse within the particles [22,60]. In the case where ammonia is injected followed by water, it is likely that more pure water and pure ammonia particles are formed by homogeneous freezing instead of core–shell particles. As said, part of the water vapour will freeze in the inlet tube and thus no longer be available for heterogeneous freezing. This results in fewer core–shell particles in comparison to the opposite injection order, and thus less mixing via solid-state diffusion. This explanation is consistent with the spectra and data in Figures 4–6. We believe that the majority of mixing occurs via solid-state diffusion after the formation of core–shell particles, although it may not be the sole mechanism for the formation of molecularly mixed particles. Collision of pure particles in the cell followed by solid-state diffusion might contribute as well. Sublimation and re-condensation of gas is not plausible considering the calculated sublimation pressures for ammonia and water of 1.3×10^{-14} bar and 5.2×10^{-27} bar, respectively (at 78 K) [62]. As we are not able to accurately quantify the properties of our particles (e.g., we do not know the interface area in the core–shell particles), we do not try to assign a rate to the mixing process observed in spectra.

3.2. *Acetylene–water aerosol particles*

3.2.1. *Overview of aerosol particle IR spectra*

We observed very similar trends for the acetylene–water aerosol particles as for the ammonia–water particles. Since the ammonia–water results have already been discussed in detail, we only briefly summarise the results for the acetylene–water aerosol particles.

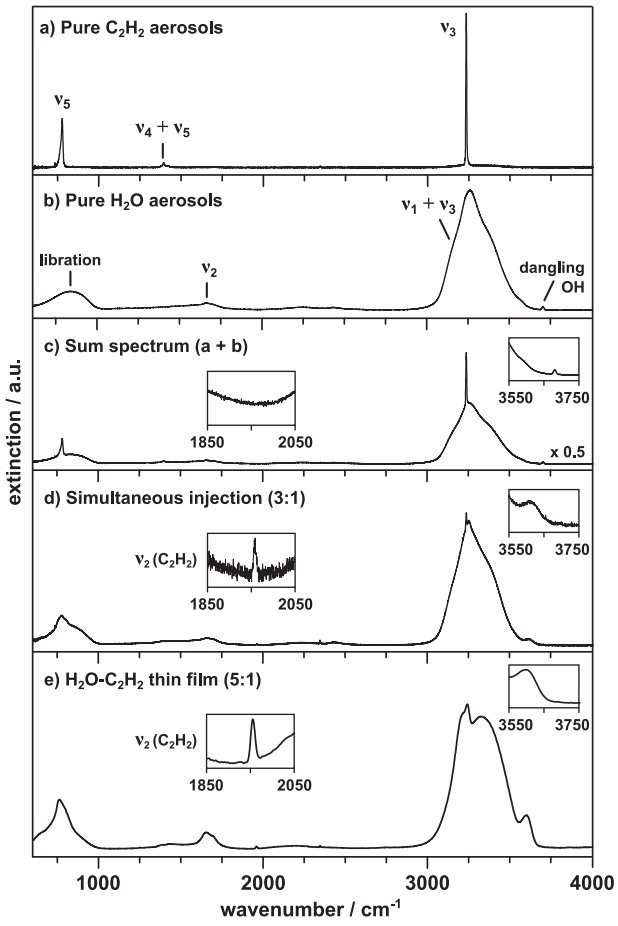

Figure 7. Overview infrared aerosol particle spectra for (a) pure C_2H_2, (b) pure H_2O, (c) a sum spectrum (addition of spectrum (a) and spectrum (b)), and (d) particles formed after simultaneous injection of C_2H_2 and H_2O samples. The ratio H_2O:C_2H_2 is approximately 3:1 in (c) and (d). (e) An H_2O–C_2H_2 (5:1) thin film measurement at 20 K. The thin film spectrum was taken from the work of Hudson and co-workers [26,60]. Insets show an expanded view of the region for the C_2H_2 ν_2 mode and the dangling-OH stretch region.

Overview IR spectra of pure and molecularly mixed solid acetylene and water aerosol particles at 78 K are shown in Figure 7. A summary of the band positions in the pure and mixed acetylene and water aerosol particle spectra is provided in Table 2. There were no significant changes observed in any of the spectra over a measurement time of 30 minutes. The spectrum of pure acetylene particles (trace (a)) most resembles that of orthorhombic polycrystalline (partially amorphous) particles [29,31,48,62,63]. Thin films of acetylene were also found to be polycrystalline at 63 K [10]. The most prominent bands in the spectrum are the ν_5 band at 773 cm^{-1} (the bending mode) and the ν_3 band at 3230 cm^{-1} (anti-symmetric CH stretching mode). We will focus the majority of our analysis of the molecularly mixed

Table 2. Infrared band assignments for pure and mixed C_2H_2 and H_2O aerosol particles formed in the cooling cell (see Figure 7).

		Position (cm^{-1})	
	Band	Pure	Mixed*
C_2H_2	ν_5	773	789‡
	$\nu_4 + \nu_5$	1390	1390‡
	ν_2	–	1958
	ν_3	3230	3231‡
H_2O	Libration	814	‡
	ν_2	1650	1653
	$\nu_1 + \nu_3$	3257	3246‡
	Dangling-OH	3698	–
Unassigned		–	3611

*Taken from spectra recorded after simultaneous injection of the sample gases.
‡H_2O and C_2H_2 overlap in this region.

acetylene–water particles on the acetylene ν_5 band due to its strong transition dipole and sensitivity to particle properties [48]. A spectrum for pure water aerosol particles is shown in trace (b). A detailed description of the corresponding bands is given in Section 3.1.1. Figure 7(c) displays a sum spectrum of pure acetylene particles (trace (a)) and pure water particles (trace (b)) with a ratio of H_2O:C_2H_2 of ~3:1. An experimental spectrum of molecularly mixed acetylene–water particles with the same H_2O:C_2H_2 ratio is shown in trace (d). It was recorded after simultaneous injection of the two sample gases into the cell. The ratio of water to acetylene was determined from integration of bands using the band strengths obtained for water [9] and acetylene [25,63] thin films, both at 10 K. (Note that due to the overlap of the major water and acetylene bands, integration was performed for the respective pure spectra with the same ratio of the two substances.)

The overlap between the most intense acetylene bands and the broad water bands in the region around 780 and 3230 cm^{-1} complicates the detection and analysis of spectral features. Nonetheless, distinct changes are observed between the pure acetylene bands and the bands of the molecularly mixed particles. The ν_5 band (which overlaps with the water libration) is broadened and its position shifts to 789 cm^{-1} for the mixed particles. The acetylene ν_3 band in the spectrum of the mixed particles appears as a narrow sharp peak on top of the broad water OH stretching band. Its position is only shifted by 1 cm^{-1} towards higher wavenumbers compared with pure acetylene particles. As seen for the ammonia–water mixed aerosol particles, the dangling-OH stretch band is not present in the mixed acetylene–water aerosol particle spectrum; however, a new shoulder at 3611 cm^{-1} appears (insets in Figure 7(d) and (e)). The origin of this band is not clear. Some suggestions are provided by Hagen *et al*. [10], e.g. shifted pure water or pure acetylene stretching absorptions. In addition, the normally IR inactive acetylene ν_2 band (C–C stretching motion) becomes active in the spectrum of the mixed particles (inset in traces (d) and (e)). This effect was previously observed in NH_3–C_2H_2 aerosol particles and was attributed to a change in the site symmetry of the C_2H_2 in the pure crystal versus the mixed state [31].

3.2.2. *Comparison to thin film spectra*

There is considerably less literature for the acetylene–water system compared to ammonia–water. There are very few studies of acetylene–water thin films and we are not aware of any other studies of acetylene–water aerosol particles. Figure 7(e) shows an example of acetylene thin film measurement from the work of Hudson and co-workers [26,59]. The spectrum in this figure is for a H_2O–C_2H_2 mixing ratio of 5:1, though their work also includes spectra for a few other ratios, all recorded at 20 K. There are many of the same features in our particle spectrum as in the thin film spectrum, which include the broadening of the acetylene ν_5 and ν_3 bands, the shoulder at approximately 3611 cm^{-1}, and an IR-active acetylene ν_2 band. These features were also visible in their 1:1 film (not shown here). Hagen *et al*. [10] and Boudin *et al*. [25] also present a spectrum for an acetylene–water thin film (ratios of H_2O:C_2H_2 = 1:2 and H_2O:C_2H_2 = 5:1, respectively), which also exhibit very similar features (not shown). In addition, the latter contribution observed splitting of the acetylene bands, likely due to different C_2H_2 configurations within the water ice matrix, as acetylene was previously shown to bind to water ice surfaces as both a proton acceptor and a proton donor [65]. It is unclear if they also detected the shoulder around 3611 cm^{-1}, as this spectral region is not shown for the mixtures. Based on these comparisons, it is likely that we form molecularly mixed aerosol particles with an amorphous structure (see below).

It is possible for acetylene to form a co-crystal with water, where water molecules form a cage around an acetylene molecule (also referred to as a clathrate hydrate) [27,64] with a ratio of H_2O:C_2H_2 equal to 46:8. Consani and Pimentel [27] measured IR spectra for thin films of the acetylene–water co-crystal, though they looked at C_2H_2–D_2O and C_2D_2–H_2O combinations to avoid overlap of the acetylene and water bands. They compared C_2D_2–H_2O spectra of deposited films (molecularly mixed) and annealed films (co-crystal) in the region of the C_2D_2 ν_3 and ν_5 bands. Both the ν_3 and ν_5 bands are much narrower and more intense for the co-crystalline structure compared with the molecularly mixed films. In addition, they observed a large blue shift (~27 cm^{-1}) for the ν_3 band and a large red shift (~30 cm^{-1}) for the ν_5 band in the co-crystal compared to pure acetylene. Our aerosols particles are not co-crystalline structures. The H_2O:C_2H_2 ratio in our work is very different from the one needed to form co-crystals and our conditions for particle formation are quite different

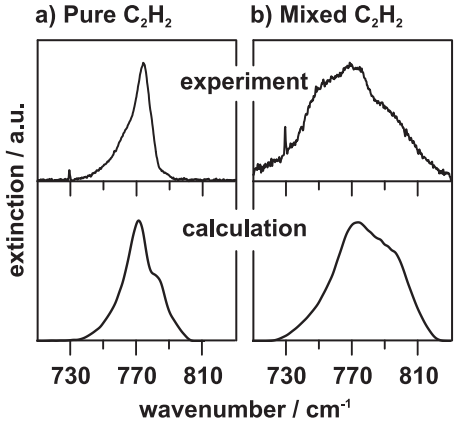

Figure 8. Comparison of experimental spectra and calculated spectra for (a) pure polycrystalline acetylene particles and (b) mixed amorphous acetylene–water aerosol particles. The calculated spectra were taken from the work of Preston *et al.* [48]. For the experimental acetylene–water spectrum, we subtracted a pure water spectrum to remove the major contributions from the broad water libration band.

from what is used to form the co-crystal. (Thin films of the acetylene–water co-crystal were formed by depositing the sample gases at 9–12 K and annealing to 130–135 K [27].) Furthermore, the band shifts observed for the co-crystal do not correspond to what we find for our C_2H_2–H_2O aerosol particles. For the aerosol particles, the ν_3 band is shifted by only 1 cm^{-1} and the ν_5 band is blue shifted and not red shifted compared to pure acetylene.

3.2.3. *Comparison to calculated spectra*

Figure 8 compares experimental and calculated spectra for aerosol particles in the region of the acetylene ν_5 band. The spectra in panel (a) are for the pure acetylene particles while the spectra in panel (b) are for mixed acetylene–water particles. (The experimental spectrum in panel (b) has had the contribution from the broad water libration subtracted to facilitate comparison to the calculated spectrum.) There is very good agreement between the experimental pure acetylene spectrum and exciton calculation for the polycrystalline particle derived from an orthorhombic structure. There is also good agreement between the experimental acetylene–water spectrum and the calculated amorphous acetylene spectrum. As for the ammonia case, the amorphous structure seems a good approximation for molecularly mixed. These calculations provide further confirmation that we form molecularly mixed acetylene–water aerosol particles with an amorphous structure.

3.2.4. *Mixing in core–shell acetylene–water particles*

Sequential injection experiments were performed for the acetylene–water aerosol particles to study mixing in core–shell particles. Over time, similar mixing trends are observed as described in Section 3.1.5 for the ammonia–water particles. Figure 9 displays time-dependent spectra after the sequential injection of first water then acetylene in the region of the acetylene ν_5 band. (This band overlaps the broad water libration band.) The ratio of H_2O:C_2H_2 is approximately 3:1, which is the same ratio as for the simultaneous injection measurement shown in Figure 7(d). Even though the overlap between the acetylene and water band complicates the analysis, there are distinct changes that can be monitored. Over time, the acetylene ν_5 band evolves from the sharp band of pure acetylene toward the broader band arising from molecularly mixed acetylene. This broadening effect is similar to what is observed for the ammonia–water aerosol particles in Section 3.1.5. In addition, we also see the following temporal evolution of other bands in the spectra (not shown): the acetylene ν_3 band broadens with time, there is a decrease in the intensity of the dangling-OH band of water, and the shoulder at 3611 cm^{-1} increases in intensity. As for the ammonia–water aerosol particles, the majority of mixing likely occurs via solid-state diffusion after the formation of core–shell particles. (The calculated sublimation pressures for acetylene at 78 K is 5.0 $\times$ 10^{-9} bar [61] which speaks against substantial contribution to mixing by

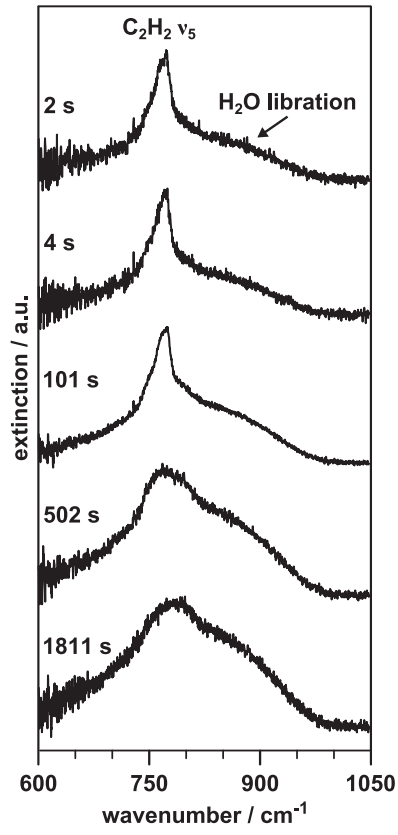

Figure 9. Temporal evolution of spectra in the region of the C_2H_2 ν_5 mode after sequential injection of the sample gases (H_2O then C_2H_2). The ratio of H_2O:C_2H_2 is approximately 3:1.

sublimation and recondensation of gas.) Again, we do not try to extract any rate constants for the mixing process because we cannot accurately quantify the properties of our particles.

4. Summary

We find that ammonia–water and acetylene–water form amorphous molecularly mixed aerosol particles in a bath gas cooling cell at 78 K. This differs from results for acetylene–carbon dioxide [29,30], ammonia–acetylene [31], and water–carbon dioxide [32] particles formed under similar conditions. The IR spectra of these particles exhibit distinct features that allow their identification and clear distinction from pure particles and mixed hydrate particles. Our studies on core–shell particles reveal fast solid-state diffusion that leads to the formation of molecularly mixed particles (on the order of a few tens of minutes). Ammonia–water and acetylene–water particles show a similar structural behaviour, which clearly differs from that of acetylene–carbon dioxide, ammonia–acetylene, and water–carbon dioxide particles (see Section 1).

Molecularly mixed ammonia–water and acetylene–water aerosol particles without any long-range order form under various conditions (e.g. various mixing ratios) and might thus be more important in planetary and lunar atmospheres than the corresponding hydrate structures. The spectra of these mixed systems are useful for the prediction of the type of aerosol particles that might be present in these atmospheres as well as for the analysis of spectra from future orbiter missions.

Acknowledgements

We would like to thank Dr Kerry Knox and Dr Kathrin Lang for assistance with experiments. Advanced computing resources were provided by West-Grid and Compute/Calcul Canada.

Funding

This work was funded by the ETH Zürich and the Swiss National Science Foundation (SNF) [grant number 200021_146368/1]; and Merrill Isenor received funding from an NSERC postgraduate scholarship and a Walter C. Sumner Memorial Fellowship.

References

[1] Ó.F. Sigurbjörnsson, G. Firanescu, and R. Signorell, Annu. Rev. Phys. Chem. **60**, 127 (2009).
[2] T.C. Preston and R. Signorell, Proc. Natl. Acad. Sci. U.S.A. **108**, 5532 (2011).
[3] T.C. Preston and R. Signorell, Acc. Chem. Res. **45**, 1501 (2012).
[4] L.A. Sromovsky, K.H. Baines, and P.M. Fry, Icarus **226**, 402 (2013).
[5] S.K. Atreya and A.-S. Wong, Space Sci. Rev. **116**, 121 (2005).
[6] A. Sánchez-Lavega, S. Pérez-Hoyos, and R. Hueso, Am. J. Phys. **72**, 767 (2004).
[7] J.H. Waite, Jr., W.S. Lewis, B.A. Magee, J.I. Lunine, W.B. McKinnon, C.R. Glein, O. Mousis, D.T. Young, T. Brockwell, J. Westlake, M.-J. Nguyen, B.D. Teolis, H.B. Niemann, R.L. McNutt, Jr., M. Perry, and W.-H. Ip, Nature **460**, 487 (2009).
[8] J.H. Waite, Jr., M.R. Combi, W.-H. Ip, T.E. Cravens, R.L. McNutt, Jr., W. Kasprzak, R. Yelle, J. Luhmann, H. Niemann, D. Gell, B. Magee, G. Fletcher, J. Lunine, and W.-L. Tseng, Science **311**, 1419 (2006).
[9] L.B. d'Hendecourt and L.J. Allamandola, Astron. Astrophys. Suppl. Ser. **64**, 453 (1986).
[10] W. Hagen, A.G.G.M. Tielens, and J.M. Greenberg, Astron. Astrophys. Suppl. Ser. **51**, 389 (1983).
[11] M.H. Moore, R.F. Ferrante, R.L. Hudson, and J.N. Stone, Icarus **190**, 260 (2007).
[12] J.E. Bertie and J.P. Devlin, J. Chem. Phys. **81**, 1559 (1984).
[13] J.E. Bertie and M.R. Shehata, J. Chem. Phys. **81**, 27 (1984).
[14] G. Sill, U. Fink, and J.R. Ferraro, J. Chem. Phys. **74**, 997 (1981).
[15] W. Zheng, D. Jewitt, and R.I. Kaiser, Astrophys. J. Suppl. Ser. **181**, 53 (2009).
[16] R.F. Knacke, S. McCorkle, R.C. Puetter, E.F. Erickson, and W. Krätschmer, Astrophys. J. **260**, 141 (1982).
[17] R.D. Waldron and D.F. Hornig, J. Am. Chem. Soc. **75**, 6079 (1953).
[18] T. Huston, I.C. Hisatsune, and J. Heicklen, Can. J. Chem. **61**, 2077 (1983).
[19] J.E. Bertie and M.M. Morrison, J. Chem. Phys. **73**, 4832 (1980).
[20] J.E. Bertie and M.M. Morrison, J. Chem. Phys. **74**, 4361 (1981).
[21] J.E. Bertie and J.P. Devlin, J. Chem. Phys. **78**, 6203 (1983).
[22] N. Uras and J.P. Devlin, J. Phys. Chem. A **104**, 5770 (2000).
[23] J.E. Bertie and M.R. Shehata, J. Chem. Phys. **83**, 1449 (1985).
[24] C. Thornton, M.S. Khatkale, and J.P. Devlin, J. Chem. Phys. **75**, 5609 (1981).
[25] N. Boudin, W.A. Schutte, and J.M. Greenberg, Astron. Astrophys. **331**, 749 (1998).
[26] C. Knez, M.H. Moore, R.F. Ferrante, and R.L. Hudson, Astrophys. J. **748**, 95 (2012).
[27] K. Consani and G.C. Pimentel, J. Phys. Chem. **91**, 289 (1987).
[28] C.F. Bohren and D.R. Huffman, *Absorption and Scattering of Light by Small Particles* (John Wiley & Sons, New York, 1983).
[29] T.C. Preston, C.C. Wang, and R. Signorell, J. Chem. Phys. **136**, 094509 (2012).
[30] T.C. Preston and R. Signorell, J. Chem. Phys. **136**, 094510 (2012).
[31] T.C. Preston and R. Signorell, Mol. Phys. **110**, 2807 (2012).
[32] M. Isenor, R. Escribano, T.C. Preston, and R. Signorell, Icarus **223**, 591 (2013).
[33] E.K. Lang, K.J. Knox, and R. Signorell, Planet. Space Sci. **75**, 56 (2013).
[34] R. Signorell, Mol. Phys. **101**, 3385 (2003).
[35] R. Signorell, J. Chem. Phys. **118**, 2707 (2003).
[36] G. Firanescu, D. Hermsdorf, R. Ueberschaer, and R. Signorell, Phys. Chem. Chem. Phys. **8**, 4149 (2006).
[37] G. Firanescu, T.C. Preston, C.C. Wang, and R. Signorell, in *Fundamentals and Applications in Aerosol Spectroscopy*, edited by R. Signorell and J.P. Reid (CRC Press, Boca Raton, 2011), pp. 25–47.

[38] A. Bonnamy, R. Georges, E. Hugo, and R. Signorell, Phys. Chem. Chem. Phys. **7**, 963 (2005).
[39] G. Firanescu and R. Signorell, J. Phys. Chem. B. **113**, 6366 (2009).
[40] G. Firanescu, D. Luckhaus, and R. Signorell, J. Chem. Phys. **125**, 144501 (2006).
[41] G. Firanescu, D. Luckhaus, and R. Signorell, J. Chem. Phys. **128**, 184301 (2008).
[42] M. Jetzki, A. Bonnamy, and R. Signorell, J. Chem. Phys. **120**, 11775 (2004).
[43] R. Signorell and M.K. Kunzmann, Chem. Phys. Lett. **371**, 260 (2003).
[44] R. Signorell, M. Jetzki, M. Kunzmann, and R. Ueberschaer, J. Phys. Chem. A. **110**, 2890 (2006).
[45] Ó.F. Sigurbjörnsson, G. Firanescu, and R. Signorell, Phys. Chem. Chem. Phys. **11**, 187 (2009).
[46] G.A. Yeo and T.A. Ford, Can. J. Chem. **69**, 632 (1991).
[47] S.K. Pope, M.G. Tomasko, M.S. Williams, M.L. Perry, L.R. Doose, and P.H. Smith, Icarus **100**, 203 (1992).
[48] T.C. Preston, G. Firanescu, and R. Signorell, Phys. Chem. Chem. Phys. **12**, 7924 (2010).
[49] A. Engdahl and B. Nelander, Chem. Phys. Lett. **100**, 129 (1983).
[50] M.K. Kunzmann, R. Signorell, M. Taraschewski, and S. Bauerecker, Phys. Chem. Chem. Phys. **3**, 3742 (2001).
[51] J.S. Holt, D. Sadoskas, and C.J. Pursell, J. Chem. Phys. **120**, 7153 (2004).
[52] M.L. Clapp and R.E. Miller, Icarus **105**, 529 (1993).
[53] F.P. Reding and D.F. Hornig, J. Chem. Phys. **19**, 594 (1951).
[54] J.P. Devlin, J. Geophys. Res. **106**, 33333 (2001).
[55] B. Rowland and J.P. Devlin, J. Chem. Phys. **94**, 812 (1991).
[56] W.J. Siemons and D.H. Templeton, Acta Crystallogr. **7**, 194 (1954).
[57] I. Olovsson and D.H. Templeton, Acta Crystallogr. **12**, 827 (1959).
[58] A.-P. Rollet and G. Vuillard, C.R. Hebd. Seances Acad. Sci. **243**, 383 (1956).
[59] The Cosmic Ice Laboratory, IR Spectra. <http://science.gsfc.nasa.gov/691/cosmicice/spectra.html>.
[60] L. Delzeit, K. Powell, N. Uras, and J.P. Devlin, J. Phys. Chem. B **101**, 2327 (1997).
[61] N. Fray and B. Schmitt, Planet. Space Sci. **57**, 2053 (2009).
[62] C.C. Wang, P. Zielke, Ó.F. Sigurbjörnsson, C.R. Viteri, and R. Signorell, J. Phys. Chem. A **113**, 11129 (2009).
[63] D.A. Dows, Spectrochim. Acta **22**, 1479 (1966).
[64] M.T. Kirchner, D. Bläser, and R. Boese, Chem. Eur. J. **16**, 2131 (2010).
[65] S.C. Silva and J.P. Devlin, J. Phys. Chem. **98**, 10847 (1994).